Journal of Ceramic Processing Research. Vol. 23, No. 3, pp. 292~297 (2022)
(Received 25 October 2021, Received in revised form 22 February 2022, Accepted 22 February 2022)
https://doi.org/10.36410/jcpr.2022.23.3.292

J O U R N A L O F
Ceramic Processing Research

Improvement of bioactivity on zirconia substrate by wollastonite slurry/spin coating

Jaeeun Go and Jong Kook Lee*
Department of Advanced Materials and Engineering, Chosun University, Gwangju 61452, Republic of Korea

Zirconia is mainly used as an implant material; however, due to bioinertness, problems, such as falling off or shaking, during implant placement arise. In this study, the bioactivity of zirconia was improved by coating the zirconia substrate with a wollastonite slurry. Suitable wollastonite slurry was prepared for spin coating by controlling the solid loading, pH, and dispersant. The surface properties of the wollastonite-coated layer, i.e., microstructural evolution, surface morphology, roughness, and phase composition, were dependent on the coating thickness, which are directly related to the number of coating cycles. The valuable wollastonite-coated layer was fabricated on the 3Y-TZP substrate by repeating the coating cycle more than four times. The wollastonite-coated layer comprised an α-phase with a porous structure, and its surface roughness increased by more than 10 times for the as-sintered 3Y-TZP substrate. The improvement in the bioactivity of the 3Y-TZP substrate by wollastonite coating was confirmed by the results obtained from *in vitro* test. During the immersion of the SBF solution, wollastonite dissolution and precipitation of hydroxyapatite particles were observed on the coated surface, indicating that the wollastonite surface coating contributed to the improvement in 3Y-TZP bioactivity.

Keywords: Wollastonite Coating, Zirconia Substrate, Slurry and Spin Coating.

Introduction

Excellent biomaterials exhibit appropriate surface chemistry and surface topology with excellent mechanical properties, which promote cell attachment, growth, and tissue formation in the body [1, 2]. Calcium phosphate- and calcium silicate-based ceramics have bioactive and biocompatible properties that are similar to natural bone tissue, which creates a desirable environment for bone regeneration and promotes direct bone bonding after implantation [3-5]. However, most bioactive ceramics have shown mechanical instability due to their dissolution into body fluids and creation of surface cracks when implanted in the human body for long ceramics have been used extensively as a period [6]. Meanwhile, zirconia and alumina femoral and dental components have excellent mechanical properties, good wear and corrosion resistance, and biocompatibility [7, 8]. However, these two ceramics possess bioinert properties; they do not directly bind to the bone during implantation, and thus, their use in medical applications has been limited [9].

Superior mechanical and biological properties could be obtained through the fabrication of biocomposite and hybrid-type implants by controlling the volume fraction and distribution of the second phase in the matrix or through the preparation of bioactive coatings on the substrate [10-12]. Bioactive surface coating is a commonly used method to enhance the bioactivity of bioinert ceramic implants [13]. As bioactive coating materials, hydroxyapatite (HA), tricalcium phosphate, and calcium silicate have been widely used for improving the bioactivity of bioinert metals or ceramics [14-16]. Among these materials, HA is mainly used for hard tissue repair because its chemical composition is similar to that of the bone [17]. However, it possesses low solubility in the body and faces low degradability [18]. Wollastonite ceramics ($CaSiO_3$) are highly bioactive and biodegradable bioceramics and can be used for bone tissue regeneration [19]. The apatite-forming ability of wollastonite is higher than that of other bioactive ceramics; however, monolithic wollastonite ceramics cannot be used in bulk due to their high degradation rate. Surface modification of wollastonite on zirconia or alumina substrates improves its biological properties and can induce the formation of apatite on the substrate surface and replacement with new bone [20].

In recent years, dental implants have often been made of structural ceramics. Zirconia is one of the most promising ceramics because it exhibits the highest mechanical toughness. However, it is considered a bioinert ceramic and only shows morphological fixation with the surrounding bone tissues when implanted without any chemical or biological bone bonding. To enable the wide biomedical applications of zirconia implants, the use of bioactive coatings on zirconia has been proposed because they combine good mechanical properties with particular bioactivity to form a strong

*Corresponding author:
Tel : +82-62-230-7202
Fax: +82-62-232-2474
E-mail: jklee@chosun.ac.kr

bond with hard and soft tissues [21].

Zirconia exhibits three different crystalline phases depending on the temperature, despite having the same chemical composition. When pure zirconia sintered above 1,500 ° is cooled, several cracks occur due to the volume expansion of the bulk undergoing a phase transformation from tetragonal to monoclinic, resulting in mechanical failure. To solve this bulk failure issue after sintering, a stabilizer was added for the tetragonal or cubic phases, which prevented the transformation to the monoclinic phase at room temperature. The crystal structure of zirconia can be determined by the amount of stabilizer added [22]. The tetragonal single phase stabilized by 3 mol% yttria is known as 3Y-TZP, and it is widely used as a dental implant material owing to its high strength and toughness, esthetics, and biocompatibility [23]. To improve the bone-bonding ability of 3Y-TZP implants, several surface modification methods have been suggested by previous studies, including surface corrosion, sandblasting, and bioactive material coating. Surface corrosion and sandblasting improve the surface roughness by generating chemical or mechanical defects, respectively. However, these methods can cause damage and defects on the implant surface [24, 25]. In contrast, surface coating with bioactive materials can prevent the formation of mechanical defects through non-machining processes [26]. Surface modification of 3Y-TZP substrates has been proposed by various methods, such as sol-gel, plasma spray, and CVD coatings [27-29]. The slurry coating process is a simple and cost-effective method that is widely used to obtain a thick coating layer and a roughened coating surface by controlling the solid loading of the slurry and the coating cycle [30, 31].

In this study, we fabricated a bioactive zirconia substrate by wollastonite surface coating and investigated the surface properties of wollastonite coatings and improved the bioactivity of the coated layer using *in vitro* tests. A slurry and spin coating method was used to prepare the wollastonite coating layer, and the solid loading in the slurry and repeated coating cycles were controlled to obtain coated layers with various thicknesses. Finally, the effects of coating parameters on the microstructural evolution, surface morphology, and phase composition were examined.

Experimental Procedure

A zirconia substrate for wollastonite slurry coating was fabricated by compaction and sintering of 3Y-TZP powder, which is a common process used for dental implant materials. The 3Y-TZP powder was prepared using a commercial TZ-3Y powder manufactured by Tosoh Company, Japan. Compaction of ceramic powder was performed with uniaxial pressing of 1 g of powder into a steel mold followed by cold isostatic pressing under a pressure of 20 MPa for 10 min. The dense 3Y-TZP substrate was obtained by sintering at 1,450 °C for 2 h.

A fluid wollastonite slurry for spin coating was prepared from commercial wollastonite powder and distilled water. Process parameters for slurry preparation were obtained from preliminary experiments. To control the fluidity and stability of the wollastonite slurry, we adjusted the slurry's pH to 12 and added 1 wt% Darvan C as a dispersant. The solid loading in the slurry, an important processing parameter, was fixed at 30 wt%, considering the forming ability of the coated layer and slurry fluidity from a preliminary experiment.

To homogenize commercial wollastonite powder, ball milling was performed for 24 h. Slurry coating was carried out using a spin coater to fabricate a uniform wollastonite coating layer. First, the zirconia substrate was fixed on the center of the spin coater and a droplet of wollastonite slurry was pipetted onto the zirconia substrate while rotating at 3000 rpm for 60 s to form a coating layer. To obtain a thick coating layer, spin coating was repeated after drying for one to six cycles. Dried specimens after final coating were densified by heat treatment at 1,350 °C for 2 h. The microstructural evolution and phase composition of the wollastonite-coated layer on the zirconia substrate were analyzed by scanning electron microscopy (SEM) and X-ray diffraction (XRD). The surface morphology was investigated by atomic force microscopy (AFM), and the surface roughness was measured from AFM images.

An *in vitro* experiment was carried out to evaluate the enhancement in the bioactivity of the wollastonite-coated zirconia substrate. After immersion of the coated specimen into an SBF solution, the dissolution and precipitation behaviors on the coated surface were investigated by SEM observation and XRD analysis. Wollastonite-coated specimens fabricated by four and six repeating coating cycles were used for *in vitro* experiments over an immersion period from 1 to 14 days. A schematic of the experimental procedure is shown in Fig. 1.

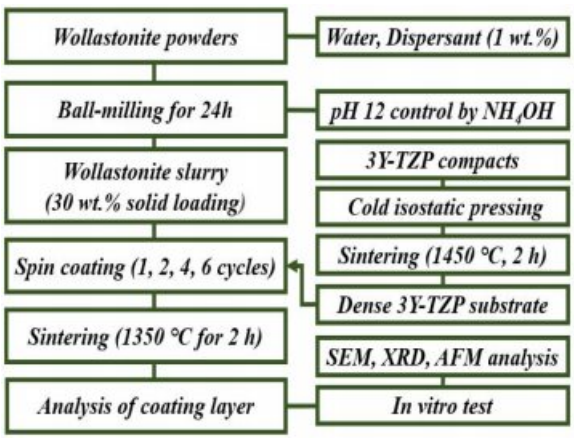

Fig. 1. Experimental procedure for slurry/spin coating of wollastonite on 3Y-TZP substrate.

Results and Discussion

The microstructure and surface morphology of the 3Y-TZP substrate for coating are shown in Fig. 2. The dense 3Y-TZP substrate was fabricated by sintering with a small grain size of 360 nm and low surface roughness of 0.04 μm. In addition, the substrate had a high sintered density (6.04 g/cm^3) and was composed of all tetragonal grains.

XRD of commercial wollastonite powder indicates a β-wollastonite phase composition, as shown in Fig. 3. Generally, natural wollastonite contains calcium silicate ($CaSiO_3$) and is produced with a mixture of low aspect ratio powder and high aspect ratio fibers, as shown in Fig. 4(a). Theoretically, wollastonite consists of 48.25% of CaO and 51.75% of SiO_2, also known as a white mineral, with a chain structure that has been used as a bioactive material in tissue repair and tissue engineering because of its bioactive and degradable properties [32, 33].

Commercial wollastonite powder used herein had a broad particle size distribution with an average particle size of 3.1 μm. Commercial wollastonite powder was ball-milled for 24 h to homogenize and reduce the wollastonite particle size. Ball-milled wollastonite powder had a smaller average particle size of 2.3 μm and a narrow particle size distribution, as shown in Fig. 4(b).

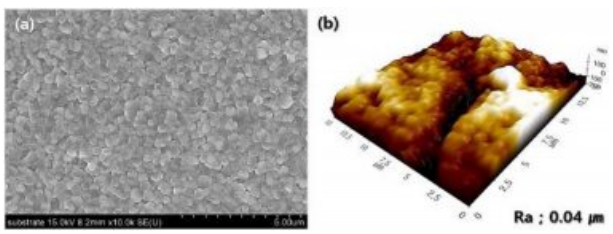

Fig. 2. Sintered characteristics of 3Y-TZP substrate for wollastonite coating: (a) surface microstructure and (b) surface morphology and roughness.

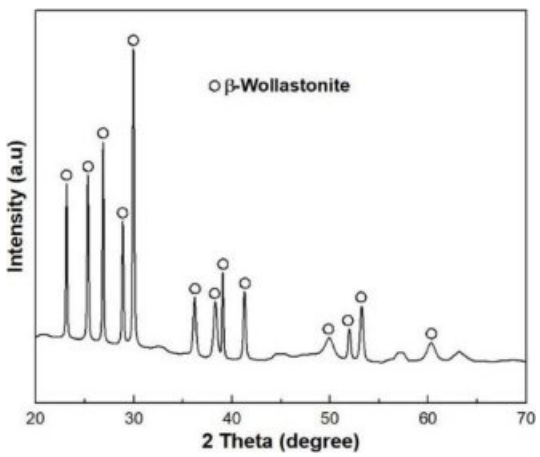

Fig. 3. Phase composition of starting wollastonite powder.

The surface microstructure of the wollastonite-coated layer after heat treatment at 1,350 °C for 2 h depends on repeated coating cycles, as shown in Fig. 5. A homogeneous coating surface on the 3Y-TZP substrate was observed by SEM for each repeated coating cycle. However, the surface morphology of the coated wollastonite particles can be clearly distinguished according to the repeated coating cycle. In the case of one or two repeated coating cycles, the wollastonite coating layer was not clearly identifiable in the microstructural observation. It was suggested that a thin coating layer with one or two repeated coating cycles was formed on the 3Y-TZP substrate by spin coating, which might have melted and absorbed into the pores on the substrate during heat treatment. In practice, the existence of small pores on the specimen surface by two repeated coating cycles was observed with a probability lower than that of one coating cycle. In contrast, for the specimen surface with four or six repeated coating cycles, the entire surface of the 3Y-TZP substrate was covered

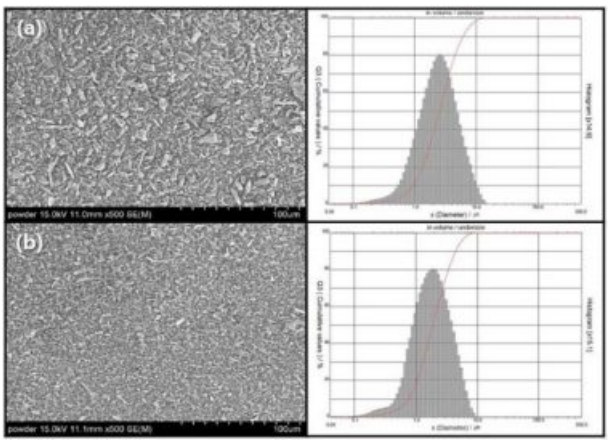

Fig. 4. Microstructure and particle size distribution of wollastonite powder: (a) commercial powder and (b) ball-milled powder for 24 h.

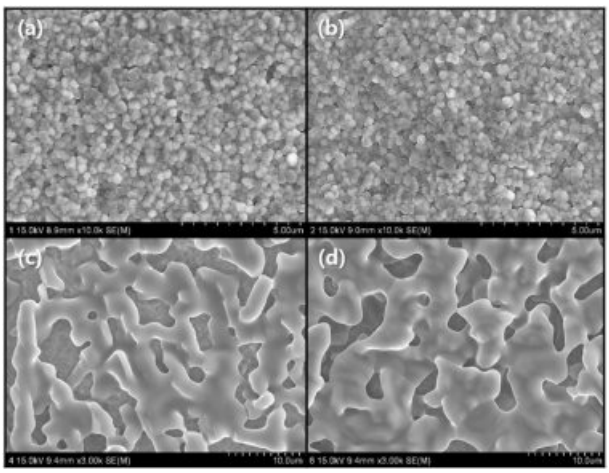

Fig. 5. Surface microstructure of wollastonite-coated layer on zirconia substrate with repeated slurry/spin coating cycle: (a) 1, (b) 2, (c) 4, and (d) 6 cycles.

with wollastonite particles with a random network structure.

To observe the interface between wollastonite and the 3Y-TZP substrate and to evaluate the thickness of the coated layer, the perpendicular microstructure of the coated layer was observed through SEM, as shown in Fig. 6. As shown in Fig. 5, an appreciable wollastonite-coated layer was not observed on the specimen surface with one or two coating cycles, as also shown in Fig. 6(a) and (b). In contrast, thick wollastonite-coated layers (4.0 and 5.9 μm) were formed on the surface of 3Y-TZP substrates with four or six coating cycles, as shown in Figs. 6(c) and (d), respectively. Wollastonite particles were uniformly attached to the 3Y-TZP substrate and a porous structure was deposited with one or two layers. The wollastonite-coated thickness and packing density of the wollastonite particles on the coating layer increased slightly with repeated coating cycles. Generally, slurry/spin coating involves a simple and inexpensive process and has the benefit of producing a thick coating layer (< 20 μm), compared to sol–gel coating method. For long-term clinical stability, slurry coating is suitable because of its thicker layer and relatively slower dissolution rate [34, 35].

Similar characteristics were investigated for the surface morphology by AFM, as shown in Fig. 7. Surface morphologies comprising small zirconia grains were observed in the wollastonite-coated surface with one or two coating cycles; accordingly, the enhancement in the surface roughness of the coated layer was insignificant compared to that in the starting 3Y-TZP substrate. In contrast, the surface morphology of wollastonite-coated specimens with four or six repeating coating cycles comprised large wollastonite grains; consequently, the surface roughness of the 3Y-TZP substrate was improved by more than 10 times.

The phase composition on the surface of the wollastonite-coated layer with repeated coating cycles was observed through XRD analysis, as shown in Fig. 8. Distinct wollastonite peaks were found on the wollastonite-coated specimens with four and six repeating coating cycles, but wollastonite peaks were insignificant or almost not observed on coated specimens with one or two repeating coating cycles. The phase composition analysis of the coated surface agreed with the micro-structural observations. Unlike the starting powder composition of β-wollastonite, the coated layer was found to be α-wollastonite resulting from a phase transition during the final heat treatment at 1,350 ºC for 2 h. Generally, wollastonite can be classified as α- or β-wollastonite, where α-wollastonite crystals have a pseudo-hexagonal structure, while β-wollastonite crystals have a triclinic structure. The β-wollastonite phase was identified by the calcination of wollastonite between 800 and 1,130 ºC, and the α-wollastonite phase was identified when the temperature exceeded 1,130 ºC [33, 36].

To confirm the enhancement in the bioactivity of

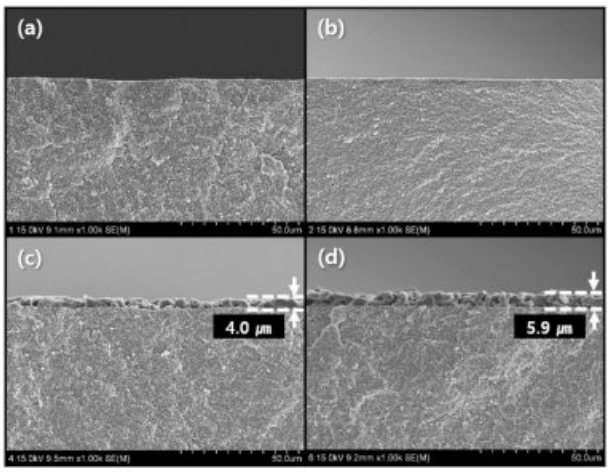

Fig. 6. Perpendicular surface microstructure of wollastonite-coated layer on zirconia substrate with repeated coating cycle: (a) 1, (b) 2, (c) 4, and (d) 6 cycles.

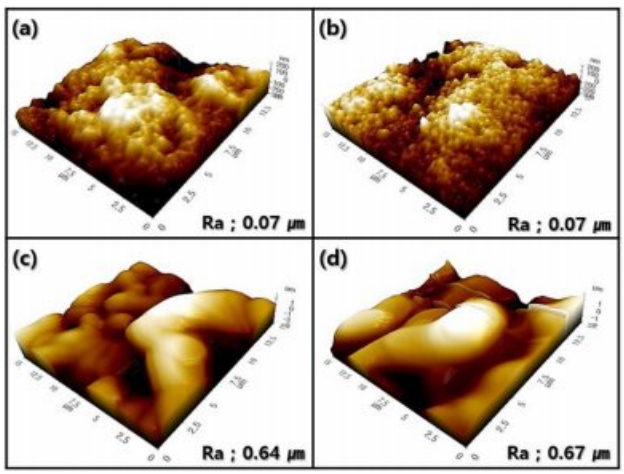

Fig. 7. Surface morphology and roughness of wollastonite-coated layer with repeated coating cycle: (a) 1, (b) 2, (c) 4, and (d) 6 cycles.

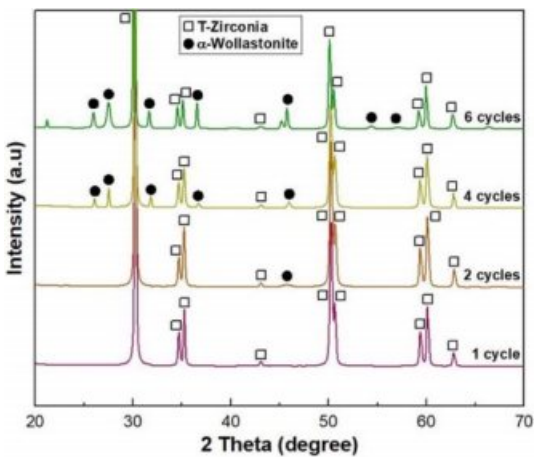

Fig. 8. Phase composition of wollastonite-coated layer with repeated coating cycle.

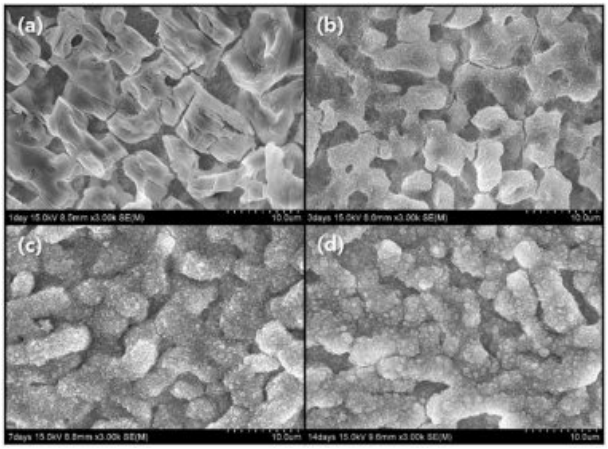

Fig. 9. Microstructural change in wollastonite-coated layer fabricated by 4 coating cycles after *in vitro* test in SBF solution with immersion period: (a) 1, (b) 3, (c) 7, and (d) 14 days.

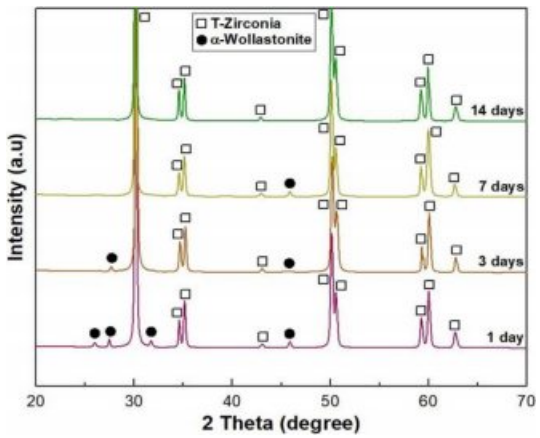

Fig. 10. Phase composition of wollastonite-coated layer fabricated by 4 coating cycles after *in vitro* test in SBF solution with immersion period.

wollastonite coating on the 3Y-TZP substrate, an *in vitro* test was performed by immersing four repeated coating specimens in SBF solution. The microstructural changes in the wollastonite-coated surface with an immersion period of 1-14 days are shown in Fig. 9. Slight surface dissolution on the wollastonite-coated surface was only observed after immersion for 1 day in the SBF solution, but after 3 days of immersion, small precipitate particles were found on the coated surface, which are expected to be HA particles. With increasing immersion period in the SBF solution, fine precipitate particles gradually grew and covered the wollastonite surface of the coating layer. The phase change in the wollastonite-coated surface with the immersion period was examined by XRD analysis, as shown in Fig. 10. The peak intensity of wollastonite gradually decreased with the immersion period in the SBF solution due to dissolution, and wollastonite peaks disappeared on the specimen surface immersed for 14 days. However, new peaks for precipitated HA particles were not found on

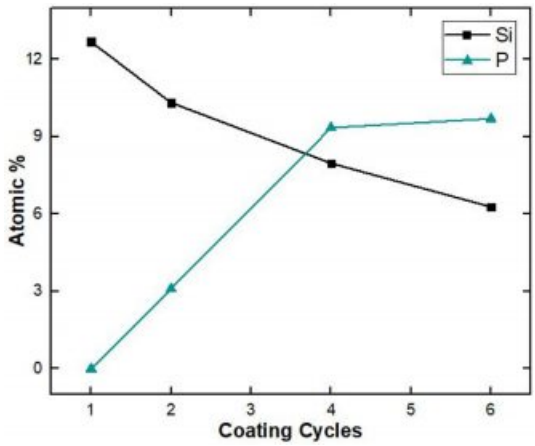

Fig. 11. EDS atomic composition on wollastonite -coated layer fabricated by 4 coating cycles after *in vitro* test in SBF solution with immersion period: (a) 1, (b) 3, (c) 7, and (d) 14 days.

the surface of the immersed specimen regardless of the immersion period.

To investigate the precipitate particles on the coated surface in an SBF solution, the change in surface composition with immersion period was examined by electron diffraction spectroscopy (EDS) analysis, as shown in Fig. 11. With an increasing immersion period, the silicon peak gradually decreased due to the dissolution of wollastonite-coated layer into the SBF solution. Meanwhile, the phosphorus peak appeared after 3 days of immersion, and increased on the specimen surface over the 14-day immersion period, indicating that precipitated HA particles from the SBF solution increased with immersion period. This result indicates that wollastonite coating can be considered a suitable method for improving the bioactivity and can be applied to dental and orthopedic implants because of the formation of apatite. In previous studies, the apatite-forming ability of wollastonite was faster than that of bioglass materials in simulated body fluids [37]. Therefore, the enhanced bioactivity of wollastonite makes it a strong candidate as an implant-coated material. Surface coating of wollastonite on 3Y-TZP is a promising method for producing excellent implant materials for medical applications.

Conclusion

To improve the bioactivity of the zirconia substrate, wollastonite was coated on the zirconia substrate by slurry and spin coating. The solid loading in the slurry and repeated coating cycles were adjusted to control the thickness of the wollastonite-coated layer. Uniform and homogeneous wollastonite-coated layers were fabricated by slurry and spin coating processes, but the valuable wollastonite-coated layer on the 3Y-TZP substrate was fabricated by repeating the coating cycle more than four times. The wollastonite-coated layer comprised α-wollastonite formed through a phase

transformation from β-wollastonite during the final heat treatment and the surface roughness enhanced by more than 10 times than that of the original 3Y-TZP substrate. The improvement in bioactivity of the 3Y-TZP substrate by wollastonite coating was confirmed through *in vitro* test. During the immersion of the SBF solution, wollastonite dissolution and precipitation of HA particles were observed on the coated surface, indicating that the wollastonite surface coating contributed to the improvement in the bioactivity of 3Y-TZP.

References

1. S. Bose, S.F. Robertson, and A. Bandyopadhyay, Acta. Biomater. 66 (2018) 6-22.
2. G. Balasundaram, and T.J. Webster, Nanomedicine. 1[2] (2006) 169-176.
3. P. Srinath, P. Abdul Azeem, and K. Venugopal Reddy, Int. J. Appl. Ceram. Technol. 17[5] (2020) 2450-2464.
4. H.Y. Song, A.H.M. Esfakur Rahman, and B.T. Lee, J. Mater. Sci.: Mater. Med. 20[4] (2009) 935-941.
5. S.V. Dorozhkin, Biomaterials. 31[7] (2010) 1465-1485.
6. Z. Abbasi, M.E. Bahrololoom, M.H. Shariat, and R. Bagheri, J. Dent. Biomater. 2[1] (2015) 1-9.
7. S. Sequeira, M.H. Fernandes, N. Neves, and M.M. Almeida, Ceram. Int. 43[1] (2017) 693-703.
8. M. Saini, Y. Singh, P. Arora, V. Arora, and K. Jain, World. J. Clin. Cases. 3[1] (2015) 52-57.
9. J. Ke, J. Ye, and F. He, ACS. Appl. Mater. Interfaces. 9[19] (2017) 16015-16025.
10. I. Karacan, I.J. Macha, G. Choi, S. Cazalbou, and B. Ben-Missan, Key. Eng. Mater. 758 (2017) 120-125.
11. Y. Yang, C. He, E. Dianyu, W. Yang, F. Qi, D. Xie, L. Shen, S. Peng, and C. Shuai, Mater. Des. 185 (2020) 108259.
12. C. Auclair-Daigle, M.N. Bureau, J.G. Legoux, and L'H. Yahia, J. Biomed. Mater. Res. A. 73A[4] (2005) 398-408.
13. K. Zhang, and Q. Van Le, J. Compos Compd. 2[2] (2020) 10-17.
14. Y. Cho, J. Hong, H. Ryoo, D. Kim, J. Park, and J. Han, J. Dent. Res. 94[3] (2015) 491-499.
15. H.W. Kim, G. George, J.C. Knowles, Y.H. Koh, and H.E. Kim, Biomaterials. 25[18] (2004) 4203-4213.
16. X. Liu, M. Morra, A. Carpi, and B. Li, Biomed. Pharmacother. 62[8] (2008) 526-529.
17. M. Akram, R. Ahmed, I. Shakir, W.A.W Ibrahim, and R. hussain, J. Mater. Sci. 49[4] (2014) 1461-1475.
18. K. Lin, M. Zhang, W. Zhai, H. Qu, and J. Chang, J. Am. Ceram. Soc. 94[1] (2011) 99-105.
19. P. Siriphannon, Y. Kameshima, A. Yasumori, K. Okada, and S. Hayashi, J. Biomed. Mater. Res. 52[1] (2000) 30-39.
20. X. Xue, X. Liu, X.B. Zheng, and C. Ding, Biomaterials. 26[17] (2005) 3455-3460.
21. J. Chevalier, and L. Gremillard, J. Eur. Ceram. Soc. 29[7] (2009) 1245-1255.
22. J. Chevalier, L. Gremillard, and S. Deville, Annu. Rev. Mater. Res. 37[1] (2007) 1-32.
23. F. Zhang, M. Inokoshi, M. Batuk, J. Hadermann, I. Naert, B.V. Meerbeek, and J. Vleugels, Dent. Mater. 32[12] (2016) e327-e337.
24. H. Sato, K. Yamada, G. Pezzotti, M. Nawa, and S. Ban, Dent. Mater. J. 27[3] (2008) 408-414.
25. R. Gruber, E. Hedbom, D.D. Bosshardt, R. Heuberger, and D. Buser, Dent. Mater. J. 31[6] (2012) 1097-1102.
26. M. Dehestani, M. Ilver, and E. Adolfsson, J. Biomed. Mater. Res. B. Appl. Biomater. 100B[3] (2012) 832-840.
27. S.D. Jin, S.C. Um, and J.K. Lee, J. Nanosci. Nanotechnol. 15[8] (2015) 5946-5950.
28. G. Wang, X. Liu, J. Gao, and C. Ding, Acta. Biomater. 5[6] (2009) 2270-2278.
29. N.M. Hwang, I.D. Jeon, L. Gueroudji, and D.Y. Kim, J. Kor. Ceram. Soc. 38[3] (2001) 218-224.
30. J. Wang, Z. Lü, K. Chen, X. Huang, N. Ai, J. Hu, Y. Zhang, and W. Su, J. Power. Sources. 164[1] (2007) 17-23.
31. W.C. Kim , and J.K. Lee, J. Ceram. Proc. Res. 21[s1] (2020) s41-s46.
32. P.N. De Aza, C.M. López, F. Guitián, and S. D. Aza, J. Am. Ceram. Soc. 76[4] (1993) 1052-1054.
33. M.Y. Zakaria, A.B. Sulong, N. Muhamad, M.R. Raza, and M.I. Ramli, Mater. Sci. Eng. C. 97 (2019) 884-895.
34. H.W. Kim, H.E. Kim, and J.C. Knowles, J. Biomed. Mater. Res. Part B: Appl. Biomater. 70B (2004) 270–277.
35. N. Ohtsu, T. Ashino, M. Ishihara, F. Sakamoto, and T. Hanawa, Mater. Trans. 48 (2007) 105-110.
36. S.H. Ahn, D.S. Seo, and J.K. Lee, J. Ceram. Proc. Res. 16[5] (2015) 548-554.
37. S. Chehlatt, A. Harabi, H. Oudadesse, and E. Harabi, Acta. Physica. Polonica. A. 127[4] (2015) 925-927.